Non-invasive water content estimation in a tuff wall by DTS

Agliata, Rosa; Bogaard, Thom A.; Greco, Roberto; Minardo, Aldo; Mollo, Luigi; Steele-Dunne, Susan C.

Citation (APA)
Agliata, R., Bogaard, T. A., Greco, R., Minardo, A., Mollo, L., & Steele-Dunne, S. C. (2019). Non-invasive water content estimation in a tuff wall by DTS. *Construction and Building Materials*, *197*, 821-829. https://doi.org/10.1016/j.conbuildmat.2018.11.250

Important note
To cite this publication, please use the final published version (if applicable).
Please check the document version above.

Non-invasive water content estimation in a tuff wall by DTS

Rosa Agliata [a,*], Thom A. Bogaard [b], Roberto Greco [a], Aldo Minardo [a], Luigi Mollo [a], Susan C. Steele-Dunne [b]

[a] *Università della Campania "L. Vanvitelli", Department of Engineering, via Roma 9, 81031 Aversa (CE), Italy*
[b] *Delft University of Technology, Department of Water Management, PO-Box 5048, 2600GA Delft, The Netherlands*

HIGHLIGHTS

- The sensitivity of a OF-DTS system to water changes in masonry materials is tested.
- An active DTS setup is used on a testing wall made of yellow Neapolitan tuff bricks.
- Acquisitions by DTS are coupled with gravimetric measurements of water content.
- The dependency of the measured temperature on water content is detected.
- Good thermal contact between cable and wall is crucial for representative readings.

ARTICLE INFO

ABSTRACT

Undesired presence of water in historical masonries has a negative effect on the walls and causes deterioration of decorative works covering the walls, such as frescoes and valuable plasters. To prevent this, non-invasive moisture measurements are needed that avoid damage during masonry inspection caused by sample taking or probe insertion. Active heated distributed temperature sensing (DTS) with optical fibres is widely used in hydrology to assess soil moisture content. The aim of this study is to examine the potential of this technique for non-invasive water content measurements in a real scale wall. The tested masonry is made of yellow Neapolitan tuff bricks, a material widely used in historical buildings of Campania (Southern Italy). Distributed temperature measurements are carried out with three different heating strategies (different power and duration) during the drying process following the complete saturation of the wall. The acquired temperature data are then processed with three different methods (estimators), so to identify the best combination of heating strategy and data processing approach. Despite the presence of a significant bias, it is possible to identify relationships between the gravimetric moisture content and the different estimators. Those relationships are influenced to a large degree by the thermal contact between the DTS cable and the masonry. This research shows it is possible to measure water content in tuff masonry using non-invasive active heated fibre optic cable when establishing good thermal contact between the cable and the masonry.

© 2018 Elsevier Ltd. All rights reserved.

1. Introduction

The healthy service life of porous building materials is affected, to a large extent, by their hydraulic properties. Indeed, these materials are able to easily absorb and retain water, the presence of which can be due to many causes, such as capillary rise, condensation and infiltration. This may result in an undesired presence of water in the building envelope, which can lead to many issues affecting the indoor life quality of the inhabitants, as well as the performances and structural health of the walls. In historical buildings, moisture presence may also result in the deterioration of the decorative works covering the barriers, such as frescoes and valuable plasters.

Although a number of methods for measuring water content in porous building materials exist [1], most of them are invasive or even destructive, and so unsuitable for masonry of historical value. Hence, there is a demand to develop completely non-invasive sensors and techniques to avoid damages caused by sample taking (i.e. gravimetric methods) and probe insertion (i.e. classical TDR and FDR techniques [2,3]). So far, many different non-invasive techniques have been tested [4], but they all have some limitations: some are not applicable in presence of magnetic fields (NMR), others are not capable of detecting small water content variations

(gamma and x-rays), their investigation depth is limited (gamma and x-rays, radar based methods), or they need access to both sides of the investigated object (microwave methods) [5]. In recent years, many studies have demonstrated that optoelectronic technologies can be successfully used in several branches of civil engineering [6], including the determination of moisture content in porous media [7–9]. One emerging technology exploiting optical fibres is Distributed Temperature Sensing (DTS), a flexible and powerful technique that provides the measurement of the temperature profile along a standard optical fibre with high accuracy and spatial resolution. DTS has been widely used in soil moisture mapping [10–14] and more recently for moisture detection in building structures with embedded optic sensors [15]. For each single acquisition, DTS is capable of registering temperature changes in each measurement point along a fibre optic cable, also of considerable length (up to several km), with high spatial (<1 m) and temporal (<1 min) resolution [10,16]. This can be useful in bridging the existing gap between point scale and wall scale measurements.

In a recent study, the potential of DTS technology for local moisture measurements in yellow tuff bricks (20 × 30 cm investigated area) was successfully tested, using a prototype probe in which 1 m fibre optic cable was embedded in a polystyrene support to ensure good contact between the cable and the wall and limit the heat dispersion [17].

The aim of this study is to examine the potential of DTS for the non-invasive mapping and monitoring of moisture in an entire wall, with high spatial-temporal resolution. A real scale wall is built with Neapolitan yellow volcanic tuff. This pyroclastic rock has been extensively used to build traditional and historical buildings in Campania region (southern Italy). Surficial DTS is done during the drying process following the complete saturation of the wall, with three different heating strategies (with different power and duration). The data are processed using three different methods to identify the best combination of heating strategy and data processing approach to maximize the sensitivity of DTS to water content variations in the wall.

2. Materials and methods

2.1. DTS operating principles

When a light beam propagates along a fibre optic cable, a part of the energy is backscattered through the cable and collected by a control unit to quantify its intensity and the elapsed time between emission and collection. As backscattering originates from any point of the cable, distributed optical fiber sensing can be used to measure deformation (e.g. [18]) and temperature along the entire cable length simultaneously. For moisture measurements, backscattering due to temperature variations is exploited [19]. It is worth noting that any heterogeneity along the cable (change of medium, density, etc.) causes a different backscattering. Most of the energy is elastically backscattered, i.e. at the same wavelength as the emitted light (Rayleigh scatter). In addition, a small fraction of the energy undergoes a less intense and inelastic scattering (Raman and Brillouin scattering). This inelastic backscatter returns signals at higher (anti-Stokes component) and lower (Stokes component) frequencies than the incident laser beam. In case of Raman scattering, the amplitude of the backscattered anti-Stokes signal depends on the cable temperature and the intensity of irradiation, while the amplitude of the Stokes signal depends only on the intensity of irradiation. Therefore, the ratio between the intensities of anti-Stokes and Stokes components allows an estimate of the cable temperature [20,12].

DTS can be used in passive or active mode. In passive DTS, the measured temperature change is due to the spontaneous variation of the temperature conditions in the medium surrounding the cable (e.g. [12]). Thermal properties (specific heat and thermal conductivity) of porous materials are a function of the moisture content. Therefore, changes in water content result in a change of the thermal response [17]. In this study active DTS is used, a technique in which the fibre optic cable also contains an electric wire that is heated up applying an electrical current pulse and the resultant temperature change in the fibre is measured (Fig. 1).

Thus, in active DTS the measurement of the temperature change caused by the electrically generated heat pulse can be used to determine the thermal properties and hence the moisture content of the investigated medium (e.g. [13]).

2.2. Experimental setup and data collection

A wall is built using 15 bricks of yellow volcanic tuff, a pyroclastic rock with high capability of water absorption [21], extracted from a surface quarry in Quarto (50% porosity [22,23]), near Naples, southern Italy. The average dimensions of each brick are 10 × 24 × 38 cm (average volume 9.2 dm^3). The dry bulk density and the soaking ratio of the bricks are determined experimentally to be 1.33 kg/dm^3 and 24%, respectively [24]. These are consistent with the typical values for yellow Neapolitan tuff [22,23].

Bricks are placed into a 190 × 160 cm tub, constructed using a wooden frame and impermeable plastic sheets. The bricks are arranged in the form of a horizontal wall, with one of the two major surfaces lying on the ground (Fig. 1). This is to achieve a horizontally homogeneous moisture content distribution in all the bricks. Quick-setting cement is used to assemble the stones together, filling the gaps between the bricks. The assembled wall measures approximately 120 × 110 cm.

A reference sample (9.5 × 14 × 24 cm) is extracted from one brick and coated on four sides with waterproof spray to prevent lateral water evaporation, mimicking the conditions of the bricks located in the middle of the wall. The reference sample is placed in the tub beside the tested wall (Fig. 2), and used to estimate the gravimetric water content, by weighing it using an electronic balance (FKB by KERN & SOHN GmbH) with an accuracy of 0.1 g.

A length of 8 m of armoured two-fibre multi-mode 50/125 μm heatable simplex optic cable (Kaiphone Technology), with operating range of −20 ∼ +70 °C, is nailed on the upper surface of the wall. Although the use of nails to fix the cable at the wall represents an invasive procedure, aim of the measurements is to explore the possibility of measuring water content variations in the tuff by placing an OF cable on the surface. For applications to masonry with valuable surface, other non-invasive procedures will be defined to keep the cable in contact with the wall surface (e.g. simply leaning the cable against the wall and exerting some pressure). The cable is arranged so that it avoids the major surface discontinuities (e.g. differences in brick heights, large superficial pores, etc.) and a minimum bend radius of 10*r was applied to avoid step
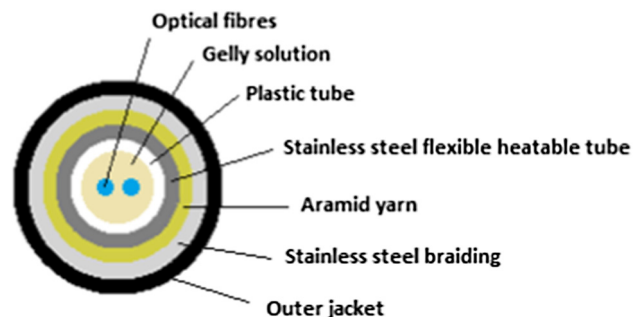

Fig. 1. Sketch of the cross section of the fibre optic cable. Radius [cm] of each layer: Outer jacket (0.30), Braiding (0.20), Aramid (0.18), Steel tube (0.16), Plastic tube (0.10), Glass fibre (0.01).

Fig. 2. Experimental setup (left) and active DTS cable layout on the tuff wall with indication of straight cable segments (right).

losses ($r = 0.3$ cm being the radius of the cable). This results in seven straight cable segments separated by curves (Fig. 2). Nails are used to ensure the contact between the cable and the wall, especially before and after each curve. In particular, at least three nails are used for each cable straight tract (two near the curves, another placed around the middle of the straight segment). For the segment closest to the sample stone, more nails are used to keep the cable in contact with the wall, since the part of the cable immediately before is in air. Clearly, the contact obtained between the cable and the wall is not homogeneous in all points of the cable; in fact, tracts where a higher number of nails is used (namely the initial portion of the first row) have a better contact than others, especially at some distance from the nails. More, at some points, i.e. immediately before the curve in the end of row 6, a better tuff/cable contact is accomplished because there the cable is embedded in the interstice between adjacent bricks.

A 2 m long cable section is also arranged to collect temperature data in air (Fig. 2). The length of the whole cable is approximately 57 m. The first and the last 15 m of cable, not affected by the heating current pulse, are coiled in a loop and laid in a calibration bath kept at constant temperature (20 °C). The temperature in the bath is registered by a thermometer probe (Fluke Calibration), connected to the machine for data collection, and served as a reference for the differential loss and temperature offset corrections. A sketch of the experimental setup is shown in Fig. 3.

Temperature data are collected using a standalone DTS unit Silixa Ultima-S (Silixa Ltd.), with an on-board PC, configured in single-ended mode. Measurements are carried out using a sampling interval of 0.127 m and a spatial resolution of 0.35 m. The temperature values are acquired by the DTS unit with a temporal resolution of 1 s and then averaged over a window of 10 s (averaging time). The sampling interval is also set at 10 s, meaning that no rest time is set between two consecutive measurements. The above parameters result in a temperature resolution of 0.11 °C. In order to identify the most sensitive experimental procedure for non-invasive moisture measurements, three different power strategies are tested across the full range of moisture values. The three strategies are designed taking into account that the temperature reached by the cable has to be compatible with the preservation of valuable walls, (e.g. integrity of fresco paints). This is essential to avoid damaging the surfaces to be preserved (e.g. colour changing). For this reason, in all the strategies the maximum temperature never exceeds 60 °C. The first heat pulse applied (S1) has the highest power input (17.4 W/m) with a duration of 5 min. This setting leads to the maximum tolerable temperature without overheating the exposed DTS cables. In the second case (S2), the applied power is reduced by one-third (11.6 W/m) and the heating duration is doubled (10 min). Finally, the lowest power input (8.1 W/m) is combined with the longest duration (15 min), denoted as S3. Heating strategies S2 and S3 have similar total injected energy (7.0 and
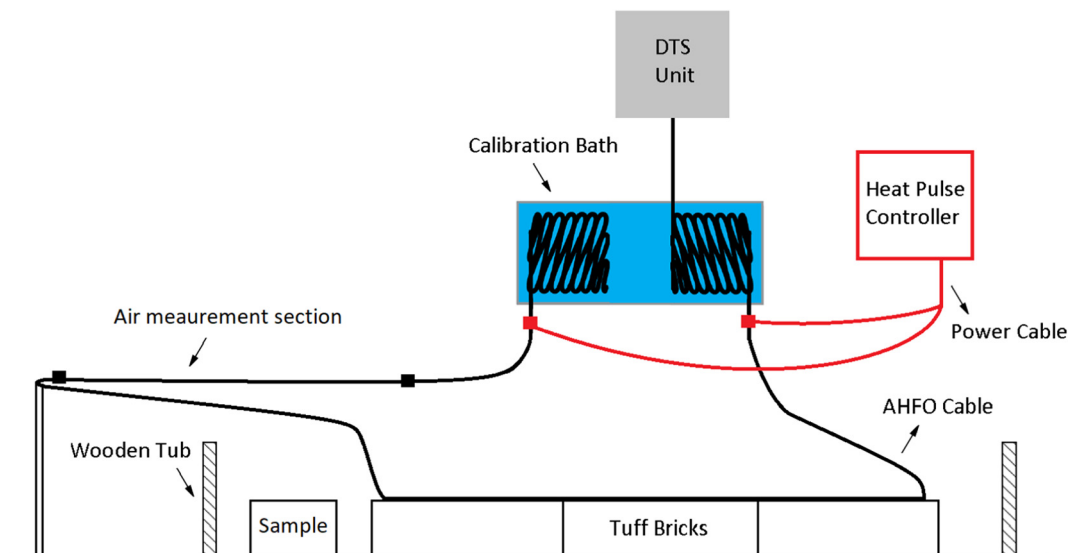

Fig. 3. Sketch of the experimental setup.

7.3 kJ/m respectively), while S1 has a significantly lower energy input (5.2 kJ/m). The current pulses are injected using a cFUSION 25 Amp controller (Control Concepts, Inc.).

The installation is placed in a controlled environment, with temperature around 20–22 °C and relative humidity around 0.5. The tub is filled with water, submerging the wall (with the cable on top of it) and the sample stone until saturation, which takes 72 h. Water is subsequently removed using a pump, and the drying phase starts. During this phase, the sample stone is weighed once or twice per day, depending on the observed drying rate, for 18 days. After this time, the wall is left drying for 45 days to achieve steady conditions (equilibrium with the surrounding environment) and finally one last measurement is acquired. During the whole experiment, every time the sample stone is weighed, DTS measurements are simultaneously made, for a total of 28 coupled acquisitions for each heating strategy.

When the experiment ends, the reference brick is subjected to a drying stage in a stove at 105 °C for 48 h. The weight of the oven-dried sample is then used as a reference to calculate its volumetric water content for each gravimetric measurement (e.g. [2]).

2.3. Moisture content estimation methods

Three different data processing methods, described below, are used to analyze point by point the temperature data collected along the cable.

The first method examines the T_{max} [°C], defined as the average of temperature data collected over a time interval, $\Delta t = 60$ s for S1 and S2 and = 120 s for S3, once the temperature rise has plateaued [25] (see Fig. 4). It is given by:

$$T_{max} = \frac{1}{n} \sum_{t_e - \Delta t}^{t_e} \Delta T(t_i) \tag{1}$$

where n is the number of measurements acquired during Δt, ΔT [°C] is the temperature increment with respect to the initial temperature and t_e [s] is the ending time of the heat pulse. The initial temperature at each point is calculated as the average of the temperature measured by DTS during the 120 s prior to the power injection.

The second method uses the cumulative temperature increase after heating, T_{cum} [°C] [13]. The latter depends on the thermal properties of the surrounding medium and is given by:

$$T_{cum} = \sum_{t_s}^{t_e} \Delta T(t_i) \tag{2}$$

where t_s [s] is the starting time of the heat pulse. It is essentially the area under the curve, as shown in Fig. 4.

In the exponential decay time method, the cooling phase after the heat pulse (see Fig. 4) is analyzed to estimate the coefficient λ [s^{-1}], called exponential decay constant, by assuming:

$$\Delta T(t) = T_{max} e^{[-\lambda(t-t_e)]} \tag{3}$$

where $\Delta T(t)$ is the temperature increase measured from the ending time of the heat pulse until the end of the measurement. The inverse of λ is a characteristic time of the heat diffusion, which depends on the thermal diffusivity of the materials surrounding the heated cable and on a characteristic length, accounting for the heat penetration depth around the heat source [26]. The exponential dependence of Eq. (3) implies that heat diffusion in the tuff around the cable is assumed to be axial symmetric. This is the same as assuming that the temperature of the considered cable section is neither influenced by the other nearby cable sections (average spacing between cable rows is about 15 cm), nor by the opposite side of the wall. As the experiments are carried out in a controlled environment and only the moisture of the tuff changes, λ is assumed to be affected only by the changes of thermal conductivity, heat capacity and density of the tuff owing to changes in its water content.

3. Results and discussion

First, the spatial distributions of the temperatures collected on tuff with the three heating strategies are analysed. Regardless the value, the spatial temperature distribution shows almost the same pattern for all the time steps and strategies. Fig. 5 reports a generalised temperature map of the wall, classifying temperatures into four groups, from 'hot' to 'cold'. It is clear that the temperature varies along the cable. The biggest difference between 'hot points' and 'cold points' was registered for S1 (>8 °C) and the smallest one for
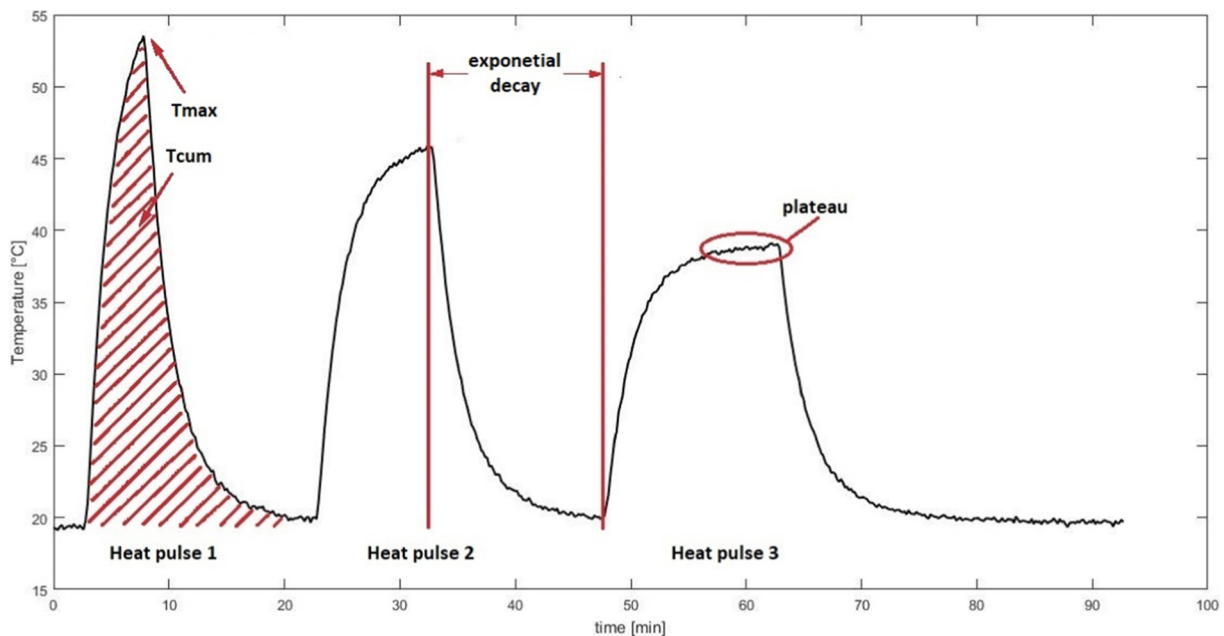

Fig. 4. Example of the temperature transients observed with the three heating strategies.

Fig. 5. Numbered measurement points (X) and temperature map. Red = hot, Orange = warm, Green = cool, Blue = cold. (For interpretation of the references to color in this figure legend, the reader is referred to the web version of this article.)

S3 (<6 °C), measured in all cases between points 29 (hottest) and 53 (coldest). The spatial distribution of temperatures along the cable remained nearly the same for all heating strategies and time steps, keeping in mind that each time step corresponds to a different water content in the wall. Clearly, the factors affecting the temperature increase along the cable section on tuff were the same at each heat pulse injection. Furthermore, the air temperature measured at the same time was almost constant along the entire cable section in air, disproving the presence of convective airflows capable of limiting the local temperature rise. Spatial heterogeneity of tuff moisture content was considered not significant, as wetter spots would result darker than drier ones, while the color of the wall surface looked fairly homogeneous during the entire experiment. Hence, the most likely cause of the spatial variations in the temperature registered along the cable section on tuff is the effectiveness of contact between the cable and the tuff. As reported in Section 2, the best tuff/cable contact was accomplished in two sections, namely from point 2 to 4 (high number of nails) and from point 51 to 54 (cable embedded between adjacent bricks). As shown in Fig. 5, these points show the lowest values in temperature, meaning that a good contact between the cable and the tuff improves heat exchange. Conversely, it is easy to imagine the presence of an air gap between the cable and the bricks in points resulting in higher temperatures. In fact, although temperature data collected along the cable section in air were systematically higher than those registered on tuff, they show great similarity with 'hot points'.

Then, the space-time distribution of T_{max}, T_{cum} and λ on tuff was examined for each heating strategy. As an example, Fig. 6 shows the space-time distributions of λ obtained using the heating strategy S1, T_{max} using S2, and T_{cum} using S3. Darker plotted curves correspond to wetter tuff. The temperature plots clearly show the persistence of cold and hot sections regardless of the adopted heating strategy and the wetness of the wall. They also highlight that at most points there is no clear trend of the calculated estimator with tuff moisture content. In some cases, the curves corresponding to

different moisture contents even cross with each other (e.g. points from 38 to 45 in T_{max}_S2 and T_{cum}_S3), which prevents linking the measured thermal parameter to the water content of the wall. The points where the temperature shows the clearest trend with water content are points from 2 to 4 and from 51 to 54 (circled in Fig. 6), thus confirming the interpretation of the cold points as those where the best heat exchange between cable and tuff is achieved. Therefore, sections from point 2 to 4 and from 51 to 54, were considered the most representative of the thermal response of wet tuff and all further reported results refer to them only.

Fig. 7 shows how T_{max}, T_{cum} and λ vary with the gravimetrically measured water content for each of the heating strategies. Each column corresponds to a heating strategy and each row to a data processing method. It is worth noting that the data collected in point 2 were not used in T_{cum} and T_{max} data processing methods.

In order to evaluate the suitability of active DTS for masonry water content measurements, both the uncertainty and the sensitivity of the measurements to water content variations have to be considered. To assess the uncertainty, the standard deviation of the measured thermal estimators is calculated. At the i-th measurement time (i-th water content), it is defined as:

$$\sigma_i = \sqrt{\frac{\sum_{j=1}^{n_i} \left(x_{i,j} - \bar{x}_i \right)^2}{n_i}} \qquad (4)$$

where $x_{i,j}$ is the j-th measured value of thermal estimator (i.e. j-th measurement of T_{max}, T_{cum} and λ) at the i-th time, $\bar{x}_i$ is the mean value of the i-th measurement, and n_i is the number of observation points selected at the i-th measurement, for each processing approach. In order to evaluate the extent to which the uncertainty affected the sensitivity of the measurement method, two dimensionless indicators have been calculated: the maximum variation coefficient $c_v = \sigma_{max}/\bar{x}_{\sigma_{max}}$, (in which $\sigma_{max} = \max\{\sigma_i\}$ is the maximum standard deviation and $\bar{x}_{\sigma_{max}}$ is the mean value of the measurement corresponding to σ_{max}) and the rangeability, evaluated as the ratio between the maximum standard deviation and the total observed range of variation (RV) of the mean measured quantity, $c_{RV} = \sigma_{max}/RV$. The smaller the values of c_v and c_{RV}, the higher the capability of the method to provide unambiguous estimates of the water content. To be able to compare the different ranges of variation, RV was normalized dividing it by the mean value of all the mean values ($RV_n = RV/\bar{\bar{x}_i}$, where $\bar{\bar{x}_i} = mean(\bar{x}_i)$). The obtained results are summarized in Table 1.

The largest spread of the measurements is generally registered for low water contents (around 15%), except for the combinations T_{max}_S1 (for which the maximum dispersion is recorded at the highest water content, θ = 0.42), λ_S2 and λ_S3 (at θ = 0.24 and 0.31, respectively).

As expected, the pulse with the highest input power (S1) produces the highest value of T_{max} (Fig. 7a). The difference in T_{max} between strategy S1 and S2 is around 6 °C, the same as between S2 and S3. The largest normalized dynamic range of values with T_{max} approach is achieved by using S2 (Fig. 7b), while the smallest with S1 (Fig. 7c). For the T_{max} method, all the strategies show similar maximum standard deviations, S1 shows the best c_v (that is also the lowest among all the combinations of heating strategy and data processing approach) and S2 the best c_{RV}.

Since T_{cum} is a measure of the total undissipated energy, similar values are reached using either the medium power input with a medium duration (S2, Fig. 7e) or the lowest power input with the longest pulse (S3, Fig. 7f). The S1 strategy, which applies the highest power but with the shortest duration, corresponds to the lowest T_{cum} values (Fig. 7d), c_v and c_{RV}, the latter being also the best among all the combinations of heating strategy and data
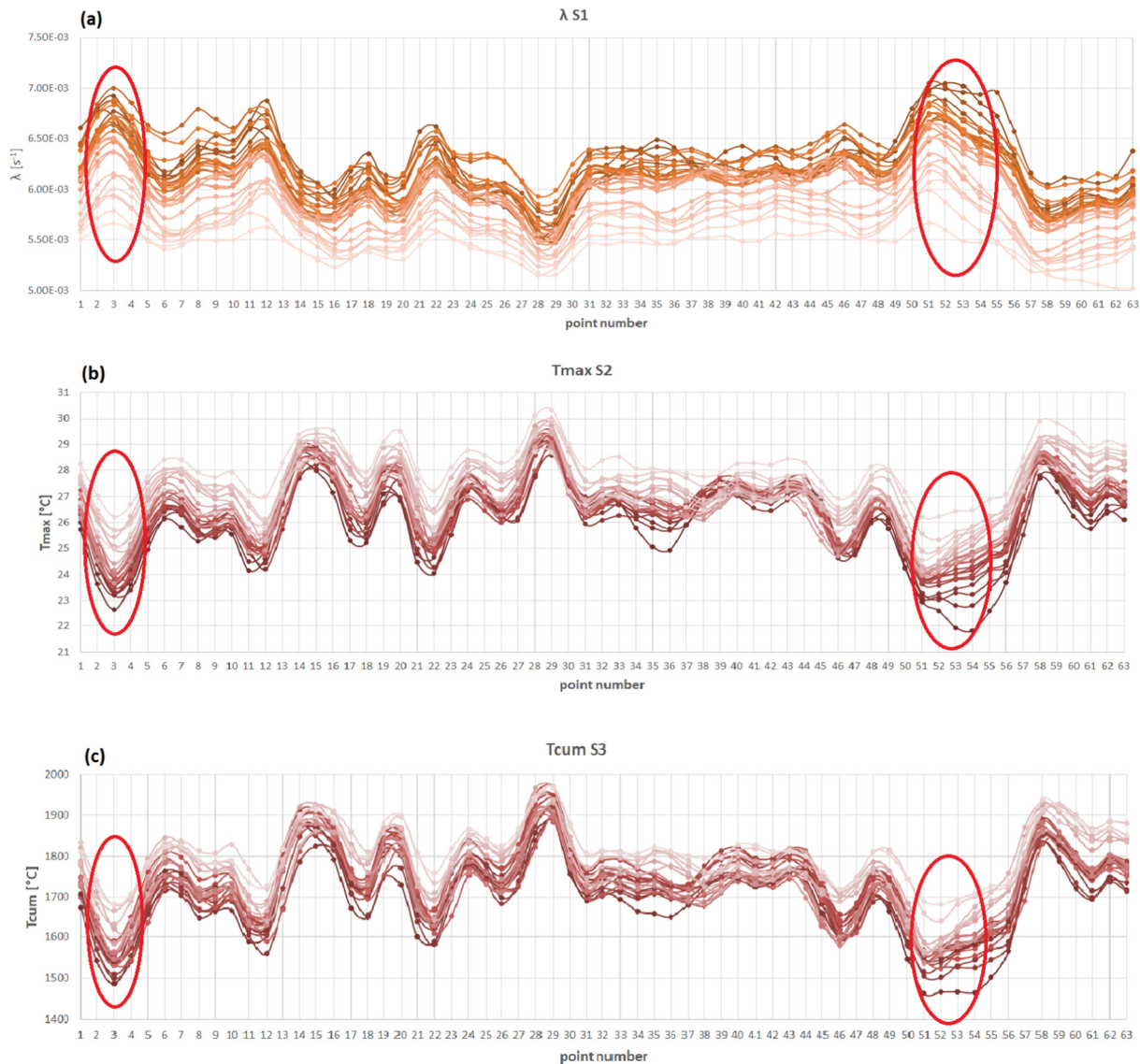
Fig. 6. Examples of space-time distribution of thermal response along the wall: (a) λ for heating strategy S1; (b) T_{max} for heating strategy S2; (c) T_{cum} for heating strategy S3. Darker curves indicate higher water contents while lighter curves are used for smaller water contents.

processing approach. T_{cum} measurements with S1 and S2 strategies exhibit similar normalized dynamic ranges of values, while S3 the smallest.

With the cooling phase analysis approach, the obtained λ values are quite similar for all the heating strategies, particularly for S1 (Fig. 7g) and S2 (Fig. 7h). These two strategies also show the same normalized dynamic range of λ values (that is also the best among all the combinations of heating strategy and data processing approach) and similar scatter, c_v and c_{RV}. Smaller range and higher dispersion are provided by S3 (Fig. 7i). This is because starting the cooling phase at higher temperature reduces the relative impact of measurement noise, providing a clearer relationship between λ and the water content. This result is consistent with a similar study on soils [10].

As heating strategy S3 corresponds in all cases to the worst c_v and c_{RV} coefficients, it has been excluded from the following discussion. Despite the low values of c_v and c_{RV}, for both T_{cum} and T_{max} approaches with heating strategy S1, the slope of the relationship between water content and temperature is nearly vertical for $\theta = 0.25$–0.37, meaning that the measured temperature could be

associated with any value of θ in that interval. Similarly, the trend of λ for the strategy S2 becomes nearly vertical for $\theta > 0.20$. Therefore, the relationships linking the measured estimator with the water content have been investigated only for the results obtained with T_{max}_S2, T_{cum}_S2 and λ_S1.

Fig. 6 shows two fitting curves (a power law and a linear regression) obtained considering all the selected points for each of the aforementioned combinations. Higher order polynomials, capable of better fitting the irregular trend shown by the experimental points (i.e. with higher R^2), have not been considered so far. In fact, the cause of this irregular trend is still not clear, and could be an artifact due to the not yet well-defined experimental procedure. Hence, the focus is on the sensitivity of the method over the entire measurement range, rather than on identifying a relationship capable of following slavishly the observed trend. Furthermore, high-order polynomial fits may lead to implausible values outside the investigated moisture range.

The T_{max}_S2 (Fig. 8a) fitting power law (pl) has a slightly higher determination coefficient than the linear regression (lr). Moreover, the latter overestimates water contents near saturation and
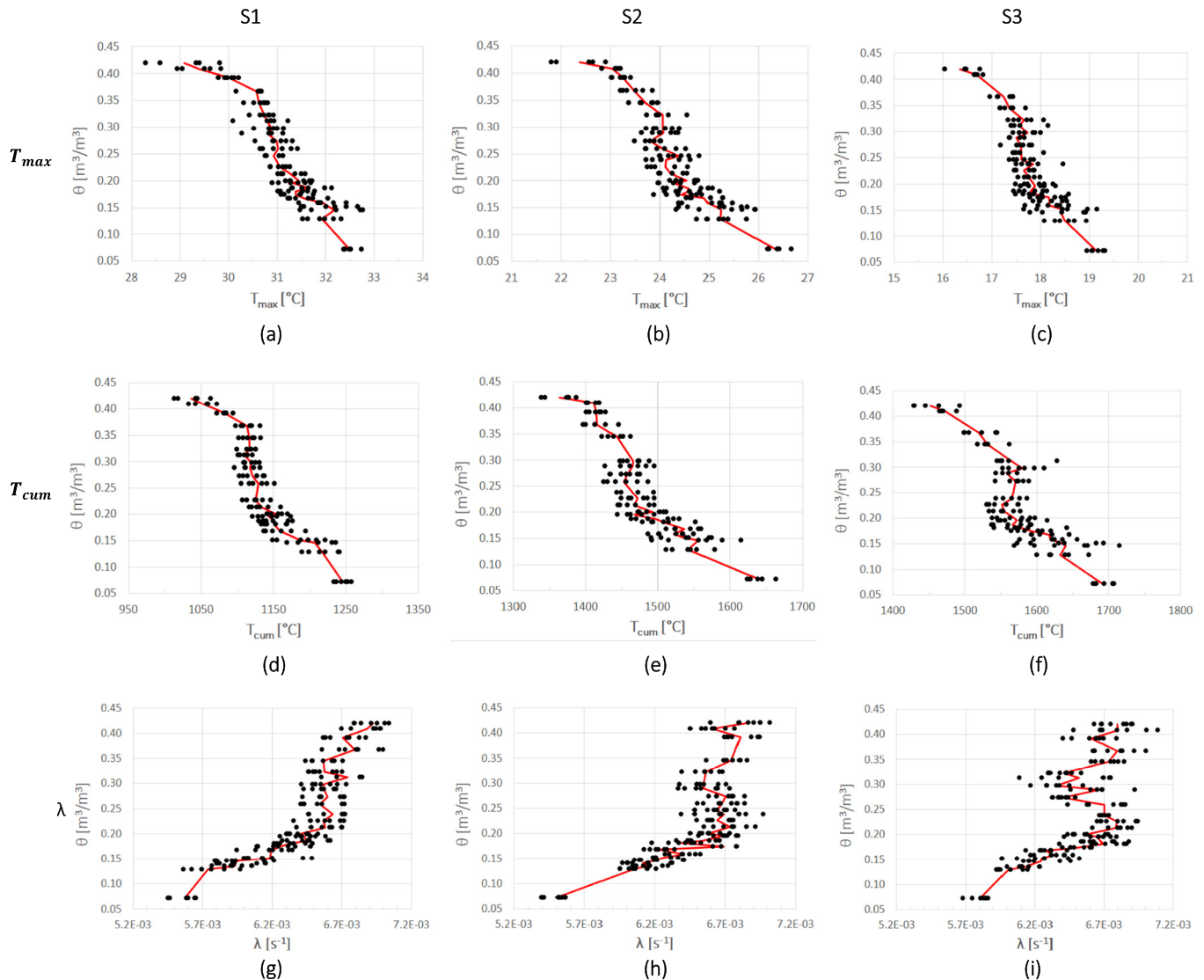
Fig. 7. Experimental dependence of tuff water content on measured thermal variables for the three adopted processing methods (rows: T_{max}, T_{cum} and λ) and the different heating strategies (columns: S1, S2 and S3). Black dots represent the experimental points; solid red lines represent the mean values in space. (For interpretation of the references to color in this figure legend, the reader is referred to the web version of this article.)

Table 1
Values of maximum standard deviation (σ_{max}), total observed range of variation (RV), maximum coefficient of variation (c_v) and rangeability (c_{RV}), for different heating strategies and water content estimators.

		S1			S2			S3		
		T_{max} [°C]	T_{cum} [°C]	λ [s^{-1}]	T_{max} [°C]	T_{cum} [°C]	λ [s^{-1}]	T_{max} [°C]	T_{cum} [°C]	λ [s^{-1}]
σ_{max}		0.56	26.79	1.87E−04	0.59	42.09	1.91E−04	0.53	49.05	2.51E−04
RV_n	[%]	10.9	18.4	21.1	16.4	18.7	21.1	15.7	15.2	15.3
c_v	[%]	1.9	2.3	3.0	2.3	2.7	2.9	2.9	3.0	3.8
c_{RV}	[%]	16.5	12.8	13.8	14.8	15.2	14.0	18.9	20.5	25.1

underestimates low water contents. The power law, instead, provides a good estimate also for low water contents, but returns physically implausible values of the water content (larger than tuff porosity) for $T_{max} < 22.8$ °C.

The T_{cum}_S2 (Fig. 8b) fitting power law behaves similarly to that of the T_{max}_S2, while the linear regression provides a good water content estimate near saturation, but again underestimates water contents under 10%. T_{max}_S2 and T_{cum}_S2 have the same determination coefficient ($R^2 = 0.76$), while T_{cum} has the highest among all tested combinations ($R^2 = 0.83$).

In the λ approach (Fig. 8c) power law fitting curve has a much higher R^2 than the linear regression, and returns reasonable estimates within the entire moisture range, while the linear fitting shows the weakest correlation ($R^2 = 0.71$) and underestimates water content both near saturation and in dry conditions.

Another important requirement of the measurement method is that the sensitivity of the estimator to water content variations should remain as high as possible within the entire measurement range. Fig. 9 shows the comparison between the sensitivity of the different combinations of heating strategy and data processing
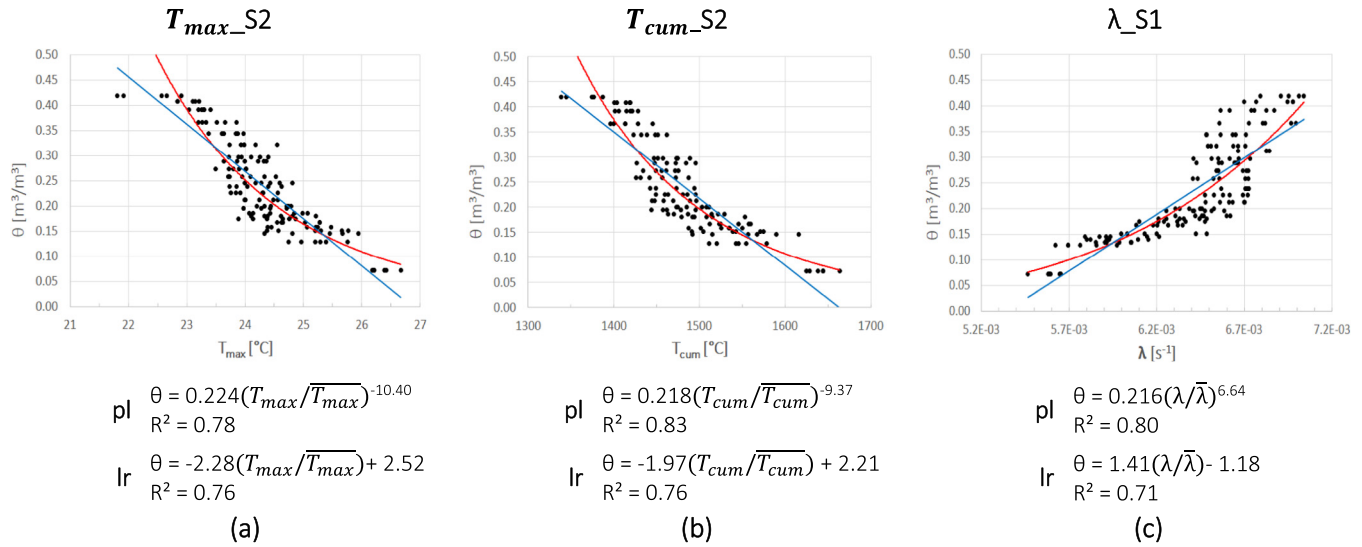
$$T_{max\_}S2 \qquad\qquad T_{cum\_}S2 \qquad\qquad \lambda\_S1$$

pl $\theta = 0.224(T_{max}/\overline{T_{max}})^{-10.40}$ pl $\theta = 0.218(T_{cum}/\overline{T_{cum}})^{-9.37}$ pl $\theta = 0.216(\lambda/\overline{\lambda})^{6.64}$
    $R^2 = 0.78$ $R^2 = 0.83$ $R^2 = 0.80$

lr $\theta = -2.28(T_{max}/\overline{T_{max}}) + 2.52$ lr $\theta = -1.97(T_{cum}/\overline{T_{cum}}) + 2.21$ lr $\theta = 1.41(\lambda/\overline{\lambda}) - 1.18$
    $R^2 = 0.76$ $R^2 = 0.76$ $R^2 = 0.71$

(a)   (b)   (c)

Fig. 8. Fitting curves of T_{max}, T_{cum} and λ as a function of water content for S1 and S2 heating strategies. Black dots indicate experimental values. Solid lines represent the fitting curves: red is for the power law (pl) and blue for the linear regression (lr). T_{max}, T_{cum} and $\overline{\lambda}$ indicate the mean value of all the measurements for each estimator. (For interpretation of the references to color in this figure legend, the reader is referred to the web version of this article.)
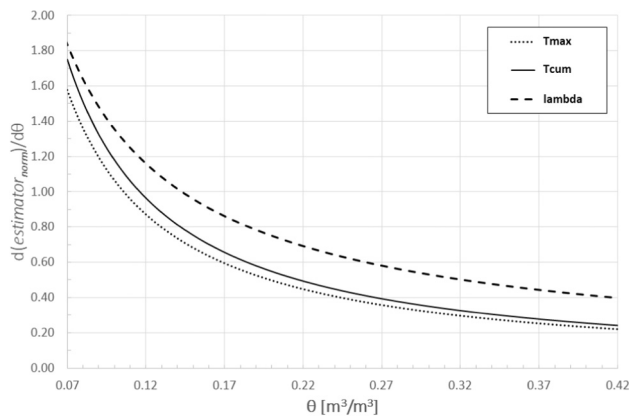

Fig. 9. Sensitivity of the power laws to water content. Curves are derived from the fitted relationships in Fig. 8.

approach for the power law-fitting, while for the linear regression the derivative, and thus the sensitivity, are constant with the water content. Aiming to compare the different sensitivities, the derivative d($estimator$)/dθ has been normalised, dividing it by the mean value of all the measured values for each estimator. For both the power law fitting and the linear regression, the λ approach shows the highest sensitivity (0.71 for lr) and T_{max} the lowest (0.44 for lr, while the sensitivity of T_{cum} for lr is 0.51). Regarding the power law fitting, the combination $T_{cum\_}S2$ has slightly higher sensitivity than $T_{max\_}S2$ and the difference between the two reduces with increasing water content. Conversely, the sensitivity of λ_S1 is similar to that of $T_{cum\_}S2$ method for low values of θ, then grows with water content and finally stabilizes around $\theta = 0.15$. For all the three combinations, the sensitivity of the power fitting is higher than the one of the linear regression for water contents up to $\theta = 0.22$. Above this value, the linear regressions result more sensitive than the power laws.

In view of the above considerations, the combination providing the strongest relationship between the estimator and the water content seems to be λ_S1. This choice would be preferable also because λ is directly linkable to the thermal properties of the investigated wall. Among the temperature-based combinations,

$T_{cum\_}S2$ is preferable as it has better RV_n, R^2 and sensitivity compared to $T_{max\_}S2$.

To summarize, it seems that the major factors affecting the relationship between the measured temperature transients and the water content are the maximum temperature reached during the heating and the power of the applied current pulse. Thus, increasing the input power is effective in reducing measurement errors and the irregular variability of the obtained relationship. It is worth to note that, with strategy S1, the pulse length was too short to reach the plateau temperature, which happened instead with S2 and S3 (Fig. 4). This is probably the reason why, for S2, it was possible to directly link the temperature with the water content. As already explained in the previous section, it was not possible to apply a pulse longer than 5 min at the same power used in strategy S1, as too high a temperature would be reached. Nonetheless, the high input power allowed to establish a robust relationship between λ and the water content.

The pulse duration has probably some influence on the measurements, as found in a previous study on soils [10]. However, to evaluate such influence, pulses with the same power input and different durations should be compared.

4. Conclusions

This study investigated the potential of active DTS for non-invasive water content measurements in a real scale wall made with yellow Neapolitan tuff bricks, along which a 8.5 m long active DTS cable was applied. The impact of the heating strategy (heating pulse power and duration) on the performance of three approaches commonly used to estimate moisture using active DTS (i.e. maximum temperature, T_{max}; cumulative temperature, T_{cum}; and time constant, λ, of the exponential cooling phase) was examined, in order to identify the best performing combination of heating strategy and data processing method. In this experiment, the DTS cable was attached to the masonry using small nails at regular intervals. The difficulty of establishing good thermal contact with the wall surface along the entire cable causes the results to be representative of only some selected cable sections, where a good heat exchange was achieved. This highlights the importance of accomplishing a good contact between the FO cable and the wall surface to obtain representative readings. This experiments shows the

potential of active DTS for moisture estimates in walls, but the obtained results are only valid for the adopted experimental procedure (i.e. nailing the cable on the wall). Therefore, future work should focus on the definition of a non-invasive and controlled procedure to establish an effective thermal contact.

The obtained results show that increased power input improves the precision of all three processing methods. A short pulse with high power has the advantage of the lowest measurements scatter for all processing methods but, in temperature-based approaches, it shows insufficient sensitivity. A medium pulse duration with medium power provides the widest dynamic range of T_{max}, T_{cum} and λ values across the moisture content variation but, in the cooling phase analysis, it shows worse sensitivity than the first described heating strategy. A long pulse with low power, though having the largest injected energy and the longest pulse, results the low rise in temperature and is therefore the least effective in all cases.

Although significant bias affected the measurements, it was possible to detect a relationship between the gravimetrically measured water content and the estimators T_{max}, T_{cum} and λ, for at least one heating strategy for each data processing method. Furthermore, the sensitivity of the identified relationships might be improved by using a support of insulating material. This would allow the application of a slight pressure to ensure adherence of the cable to the wall. This would prevent the use of nails and enhance the effective heat exchange by limiting the effect of external dynamic sources of uncertainty (i.e. convective airflows). This aspect will be the focus of future research.

In conclusion, active DTS represents a promising indirect technique for measurements of water content in porous building materials and, thanks to its possible non-invasive applicability, it can be considered a potentially suitable method also for valuable masonry elements in heritage buildings. Further research will investigate the moisture distribution across the thickness of the bricks, both experimentally (e.g. using layers of OF cable placed at different depths from the surface of the bricks, and coupling the temperature measurements with independent moisture measurements, like TDR acquisitions), and mathematically (e.g. carrying out inverse numerical modelling of the heat diffusion around the cable).

Acknowledgments

References

[1] M.C. Phillipson, P.H. Baker, M. Davies, Z. Ye, A. McNaughtan, G.H. Galbraith, R.C. McLean, Moisture measurement in building materials: an overview of current methods and new approaches, Build. Serv. Eng. Res. Technol. 28 (4) (2007) 303–316.

[2] L. Mollo, R. Greco, Moisture measurements in masonry materials by time domain reflectometry, J. Mater. Civ. Eng. 23 (4) (2010) 441–444.

[3] R. Agliata, L. Mollo, R. Greco, Use of TDR to compare rising damp in three tuff walls made with different mortars, J. Mater. Civ. Eng. 29 (4) (2016) 04016262.

[4] R. Agliata, R. Greco, L. Mollo, Moisture measurements in heritage masonries: a review of current techniques, Mater. Eval. 76 (11) (2018) 1468–1477.

[5] M. Ghandehari, C.S. Vimer, I. Ioannou, A. Sidelev, W. Jin, P. Spellane, In-situ measurement of liquid phase moisture in cement mortar, NDT & E Int. 45 (1) (2012) 162–168.

[6] W.R. Habel, K. Krebber, Fiber-optic sensor applications in civil and geotechnical engineering, Photon. Sens. 1 (3) (2011) 268–280.

[7] K. Bremer, M. Wollweber, S. Guenther, G. Werner, T. Sun, K.T.V. Grattan, B. Roth, Fibre optic humidity sensor designed for highly alkaline environments, in: 23rd International Conference on Optical Fibre Sensors, International Society for Optics and Photonics, 2014, p. 9157A4.

[8] L. Alwis, T. Sun, K.T.V. Grattan, Optical fibre-based sensor technology for humidity and moisture measurement: Review of recent progress, Measurement 46 (10) (2013) 4052–4074.

[9] T.L. Yeo, T. Sun, K.T.V. Grattan, Fibre-optic sensor technologies for humidity and moisture measurement, Sens. Actuators A 144 (2) (2008) 280–295.

[10] J. Dong, R. Agliata, S.C. Steele-Dunne, O. Hoes, T. Bogaard, R. Greco, N. van de Giesen, The impacts of heating strategy on soil moisture estimation using actively heated fiber optics, Sensors 17 (9) (2017) 2102.

[11] H. Xiao, J. Huang, Experimental study of the applications of fiber optic distributed temperature sensors in detecting seepage in soils, Geotech. Test. J. 36 (3) (2013) 360–368.

[12] S.C. Steele-Dunne, M.M. Rutten, D.M. Krzeminska, M. Hausner, S.W. Tyler, J. Selker, N.C. Van de Giesen, Feasibility of soil moisture estimation using passive distributed temperature sensing, Water Resour. Res. 46 (3) (2010).

[13] C. Sayde, C. Gregory, M. Gil-Rodriguez, N. Tufillaro, S. Tyler, N. van de Giesen, J. S. Selker, Feasibility of soil moisture monitoring with heated fiber optics, Water Resour. Res. 46 (6) (2010).

[14] T. Ren, T.E. Ochsner, R. Horton, Z. Ju, Heat-pulse method for soil water content measurement, Soil Sci. Soc. Am. J. 67 (6) (2003) 1631–1634.

[15] D. Hruby, T. Kajnar, S. Kepak, J. Jaros, J. Nedoma, M. Fajkus, et al., Masonry moisture measurement using the distributed temperature sensing system, in: Fiber Optic Sensors and Applications XIV, International Society for Optics and Photonics, 2017, p. 1020814.

[16] J.S. Selker, L. Thévenaz, H. Huwald, A. Mallet, W. Luxemburg, N. Van De Giesen, M.B. Parlange, Distributed fiber-optic temperature sensing for hydrologic systems, Water Resour. Res. 42 (12) (2006).

[17] A. Minardo, E. Catalano, L. Zeni, R. Agliata, R. Greco, L. Mollo, Measurement of moisture content in masonry materials by active distributed optical fiber sensors, in: Photonic Technologies (Fotonica 2016), 18th Italian National Conference on, IET, pp. 1–3.

[18] E. Damiano, B. Avolio, A. Minardo, L. Olivares, L. Picarelli, L. Zeni, A Laboratory study on the use of optical fibers for early detection of pre-failure slope movements in shallow granular soil deposits, Geotech. Test. J. 40 (4) (2017) 529–541.

[19] F. Ciocca, I. Lunati, N. Van de Giesen, M.B. Parlange, Heated optical fiber for distributed soil-moisture measurements: a lysimeter experiment, Vadose Zone J. (2012) 11(4).

[20] S.W. Tyler, J.S. Selker, M.B. Hausner, C.E. Hatch, T. Torgersen, C.E. Thodal, S.G. Schladow, Environmental temperature sensing using Raman spectra DTS fiber-optic methods, Water Resour. Res. 45 (4) (2009).

[21] R. Bowen, Geology and the conservation of antique monuments in Turkey, Environ. Geol. Water Sci. 9 (2) (1987) 71–84.

[22] A. Colella, D. Calcaterra, P. Cappelletti, C. Di Benedetto, A. Langella, L. Papa, A. Perrotta, C. Scarpati, M. De Gennaro, Il tufo giallo napoletano, in: M. De Gennaro, D. Calcaterra, A. Langella (Eds.), Le Pietre Storiche della Campania dall'oblio alla Riscoperta, Luciano Editore, Napoli, Italy, 2013, pp. 129–154.

[23] L. Papa, I tufi vulcanici nel costruito storico: Vulnerabilità e possibili trattamenti per la conservazione e il restauro (Doctoral thesis), Università degli Studi di Napoli Federico II, Napoli, Italy, 2011.

[24] R. Agliata, T.A. Bogaard, R. Greco, L. Mollo, E.C. Slob, S.C. Steele-Dunne, Non-invasive estimation of moisture content in tuff bricks by GPR, Constr. Build. Mater. 160 (2018) 698–706.

[25] A.M. Striegl, S.P. Loheide II, Heated distributed temperature sensing for field scale soil moisture monitoring, Ground Water 50 (2012) 340–347.

[26] T.L. Bergman, A.S. Lavine, F.P. Incorpera, D.P. Dewitt, Fundamentals of Heat and Mass Transfer, John Wiley and Sons, 2011, p. 1048.